Towards a comprehensive understanding of molecular cloud life cycle based on Hı observations with the ngVLA

Masato I.N. Kobayashi, [1] Kazuki Tokuda, [2,3]

[1]*Astronomical Institute, Graduate School of Science, Tohoku University, Aoba, Sendai, Miyagi 980–8578, Japan*

[2]*Department of Physical Science, Graduate School of Science, Osaka Prefecture University, 1–1 Gakuen–cho, Naka–ku, Sakai, Osaka 599–8531, Japan*

[3]*National Astoronomical Observatory of Japan, 2–21–1 Osawa, Mitaka-shi, Tokyo 181–8588, Japan*

mskobayashi@astr.tohoku.ac.jp, masato.kobayashi@nagoya-u.jp

Abstract

Molecular cloud formation and evolution is a key initial condition of galactic star formation. The understanding of star formation and subsequent galaxy evolution needs to reveal how the galactic environments and the driving mechanisms of cloud life cycle govern the molecular cloud properties and star formation processes. Recent observational and theoretical studies suggest that the inner structures of molecular clouds (e.g., supersonic turbulence, filaments and hubs) are the imprints of formation conditions/mechanisms of molecular clouds. In particular, the multiphase structures of molecular clouds and their precursor, Hı gas, are important to create such turbulence, filaments, and hubs, where Hı gas is often the predominant gas reservoir for molecular cloud formation in massive spiral galaxies like the Milky Way. High-resolution and high-sensitivity investigations of Hı gas make significant progress to our understanding of the origin and lifetime of molecular clouds. In this memo, we briefly summarize the importance of Hı gas observations, review recent observational and theoretical progress of molecular cloud formation, and describe our expectations to the next generation Very Large Array (ngVLA) to investigate the density and turbulence structures of Hı gas across various galactic environments.

Key words: ISM: clouds — ISM: structure — ISM: kinematics and dynamics

1. Introduction

Star formation is one of the central phenomena driving the thermal, chemical, and kinematical evolution of galaxies. In this galactic context, star formation involves various physical processes on a wide dynamic range from tens of kpc down to sub-pc scales; e.g., gas accretion and outflow between halos and galactic disks (Tumlinson et al., 2017), condensation from the diffuse interstellar medium (ISM) into molecular clouds (Baba et al., 2017), the densest part of clouds collapse to form stars (Larson, 1969) *etc.*. Since molecular clouds are on the size of a few pc scales and are the formation sites of stars (Kennicutt & Evans, 2012), revealing the formation and evolution of molecular clouds bridge the galaxy evolution ($\gtrsim 1$ Gyr) and the individual star formation ($\lesssim 10$ Myr).

The interstellar medium (ISM) has the multiphase structure; e.g., warm neutral medium (WNM), thermally unstable neutral medium (UNM) cold neutral medium (CNM), and molecular gas. The thermal instability plays a role controlling these phase balances (Field, 1965; Wolfire et al., 1995). The phase transitions from the WNM to UNM/CNM is believed to be triggered by supersonic shocks by supernovae (e.g., McKee & Ostriker, 1977), superbubbles (e.g., McCray & Snow, 1979), galactic spirals (e.g., Kim, Kim, & Ostriker, 2020), and galaxy mergers (e.g., Heitsch et al., 2006). To understand how star formation appears along with galaxy evolution, it is important to reveal how the development of these structures in the shock-ISM interacting systems depend on the galactic environments, and how they control the inner structures of molecular clouds.

Radio and infrared observations have shown the various in-

ner properties/structures of molecular clouds in detail, such as a supersonic turbulence (Heyer & Dame, 2015), filamentary structures (André et al., 2010), and hub structures connecting filaments (Kumar et al., 2020). Meanwhile, recent numerical simulations suggest that these rich structures are the imprints of formation conditions/mechanisms of molecular clouds. For example, the supersonic motion with respect to molecular gas is subsonic with respect to the WNM. Therefore, turbulent WNM in the shock downstream maintain the supersonic motion of molecular gas (Koyama & Inutsuka, 2002). A shock-compressed molecular clouds tend to host filamentary structures (e.g., Inoue & Inutsuka, 2012; Iwasaki et al., 2019) and magnetized cloud-cloud collisions induce the formation of massive filaments through shock and magnetic field interactions (Inoue et al., 2018), whose filament structure and dynamics resemble the massive star formation at the hub point of collapsing filaments (Peretto et al., 2013). These simulations and their synthetic observations suggest that the molecular clouds are not purely molecule but essentially the mixture of the WNM, UNM, CNM, and dense molecular gas (Valdivia et al., 2016; Tachihara et al., 2018b). Therefore, in addition to ordinary molecular line surveys to probe molecular gas, observations of WNM and CNM will be crucial to understand the thermal, dynamical, and chemical evolution of molecular clouds.

Hı gas is often the predominant gas reservoir for molecular cloud formation in massive spiral galaxies like the Milky Way. Recent observations also give some hints of the rapid formation of molecular clouds and stars due to Hı gas accretion and collision, in the outskirt of the Milky Way disk and
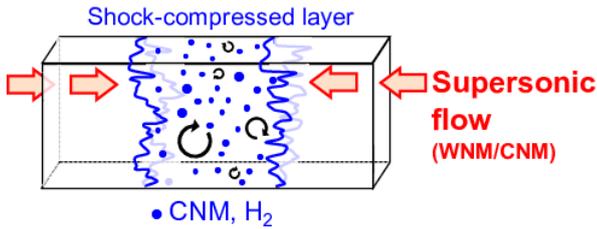
Fig. 1. Schematic figure of three-dimensional converging flow simulations (revised from Kobayashi et al. (2020)). Supersonic flows are continuously injected from the left and right boundaries. The inject flow can be purely WNM (e.g., Hennebelle et al., 2008) or the already mixture of WNM and CNM (e.g. Inoue & Inutsuka, 2012). The turbulent shock-compressed layer at the center is sandwiched by two shock fronts (black curled arrows in blue solid curves). The thermal instability develops and CNM and molecular gas form within the layer (blue points).

Large/Small Magellanic Clouds (Izumi et al., 2014; Fukui et al., 2017). Although the filamentary structures seem to commonly have a typical width of 0.1 pc, the line-mass has an order of magnitude variety (André et al., 2019), and the probability distribution function of the column density in star forming regions also does (Schneider et al., 2016), it is crucial to understand the connection between the structure of WNM, CNM, molecular gas and the variety of filamentary structures.

Therefore, the comprehensive understanding of molecular cloud life cycle across various galactic environments requires the understanding of the background HI gas reservoir together with molecular clouds. The volume of HI is dominated by WNM and UNM than by CNM (e.g., Fukui et al., 2018; Kobayashi et al., 2020). However, current observations of such detailed analysis is mostly limited to the emission-absorption feature in the line of sight against radio continuum sources, which is more sensitive to CNM (e.g., Arecibo; Heiles & Troland, 2003a,b). Therefore, it is promising that the capability of the next generation Very Large Array (ngVLA) advance our understanding of such HI structures by covering all the phases of HI gas.

In the following sections, we will review the results from recent numerical simulations (by mainly introducing our simulations (Kobayashi et al., 2020)), and express the importance/expectations to investigate the properties of HI gas in both microscopic and macroscopic viewpoints.

2. Brief review of converging flow simulations

Many previous studies have investigated the dynamical condensation through the thermal instability in a shock-compressed layer. This layer is formed by supersonic converging flows, which is a technical analog to easily calculate the thermal instability in the postshock rest frame (Hennebelle & Pérault, 1999; Koyama & Inutsuka, 2000; Heitsch et al., 2006; Vázquez-Semadeni, 2006; Inoue & Inutsuka, 2008). Figure 1 shows a schematic figure of such converging flow simulations. Two supersonic flows collide with each other at the center of the computational domain and form a turbulent shock-compressed layer. The thermal instability creates denser struc-

tures (CNM and molecular clumps) through the radiative cooling, which is mostly controlled by the Lyα and C$_{II}$ lines in the Solar metallicity environment. The turbulence here is naturally developed either by the interaction between shocks and density inhomogeneity (Richtmyer, 1960), by the thermal instability, or by the thermal conduction (Koyama & Inutsuka, 2004; Iwasaki & Inutsuka, 2014). Although there are variety in the choice of initial conditions (e.g., the density and velocity structure of the injected flow), these series of converging flow simulations suggest that molecular clouds have multiphase structure within them; WNM, UNM, CNM, and molecular gas (Valdivia et al., 2016; Tachihara et al., 2018b). The WNM and UNM govern the thermal energy and the overall dynamics whereas the CNM and molecular gas dominate the mass and turbulent energy. Therefore, the comprehensive understanding of molecular cloud life cycle requires to probe multiphase ISM coherently from WNM to molecular gas, which is currently often limited to molecular lines. The sensitivity and angular resolution capability of the ngVLA Band 1 provides a great opportunity to coherently probe all the HI phases and to advance our understanding of molecular cloud life cycle in the Milky Way and nearby galaxies.

To prepare such ngVLA observations, numerical simulations of the multiphase ISM formation and evolution should reveal how the galactic environments impact the molecular cloud formation and how they set the initial condition of star formation. Converging flow simulations are promising in this context by filling the spatial gap between galaxy evolution and individual star formation. In particular, the latest simulations of galaxy evolution start to achieve the spatial resolution of $\lesssim 10$ pc (e.g., Baba et al., 2017) and converging-flow simulations on 10 pc scales can be utilized to provide ISM sub-grid models for large-scale simulations. However, the authors on the previous converging-flow simulations employ different implementations of perturbation that initiates the thermal instability, and the perturbation amplitudes also differ between the authors accordingly. For example, a fluctuation is introduced in the upstream flow density (e.g., Koyama & Inutsuka, 2002; Inoue & Inutsuka, 2012; Carroll-Nellenback et al., 2014), velocity (e.g., Audit & Hennebelle, 2005; Vázquez-Semadeni, 2006), or a sinusoidal interface where two flows initially contact (e.g., Heitsch et al., 2005). Therefore, it is a remaining task for converging-flow simulations to reveal the spatial resolution required for a galactic subgrid-model, and to reveal how detailed conditions of the flow impact cloud properties, under a fixed method of perturbation seeding.

3. Microscopic Viewpoint: Density structure of HI gas

As such a first step to answer the above issue, we here introduce Kobayashi et al. (2020) where we perform converging flow simulations over 3 Myr in the computational domain of $L_{x,y,z} = 20, 10, 10$ pc. We introduce an upstream density inhomogeneity $\Delta\rho_0$ as a perturbation seed, which is motivated by the fact that density inhomogeneity exists essentially on all spatial scales in the diffuse ISM (Armstrong et al., 1995), through which supersonic flows are naturally expected to expand (Inoue et al., 2012; Kim & Ostriker, 2015). While the inhomogeneity has a fixed power spectrum of the Kolmogorov spectrum
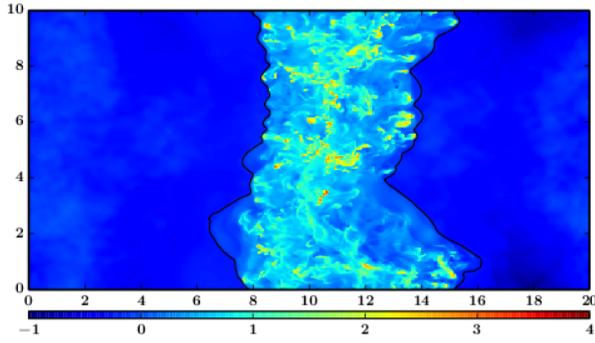
Fig. 2. The density slice from converging-flow simulations of Kobayashi et al. (2020) with $\Delta\rho_0 = 31.6\%$ at 2.2 Myr, where the color represents $\log(n[\text{cm}^{-3}])$. The horizontal and vertical axes are in the unit of pc. The thin black lines show the shock front positions.

(Kolmogorov, 1941), we systematically vary the amplitude of the upstream density fluctuation $\Delta\rho_0 = \sqrt{\langle\delta\rho_0^2\rangle}/\rho_0$ and the spatial resolution Δx to reveal the dependence of the physical properties of the multiphase ISM on those conditions. We opt to employ $\rho_0/(\mu_M m_p) = 0.57$ cm^{-3} to calculate the early phase of molecular cloud formation by purely WNM flows, where μ_M is the mean molecular weight and m_p is the proton mass. We refer the readers to see Kobayashi et al. (2020) for further information of the calculation schemes and settings.

Figure 2 shows an example of the density slice, in which the turbulent multiphase structure is developed on sub-pc scales throughout the entire shock-compressed layer. We found that the shock-compressed layer shows a bimodal behavior depending on $\Delta\rho_0$. When $\Delta\rho_0 > 10$ %, the interaction between shocks and density inhomogeneity deforms the shock fronts, leading to a strong driving of the post-shock turbulence of > 3 km s^{-1}. This strong turbulence dominates the energy budget of the shock-compressed layer and prevents the dynamical condensation by cooling and the following CNM formation. The CNM mass fraction remains as ~ 45 % in 3 Myr. In contrast, when $\Delta\rho_0 \leq 10$ %, the shock fronts maintain an almost straight geometry. The CNM formation efficiently proceeds and result in the CNM mass fraction of ~ 70 %. The velocity dispersion is limited to the thermal-instability mediated level of ~ 2–3 km s^{-1}. The shock-compressed layer is supported by both turbulent and thermal energy equally. We show that the level turbulence when $\Delta\rho_0 > 10$ % is as strong as the one expected from the interaction between shocks and density inhomogeneity (e.g., the growth velocity of the Richtmyer–Meshkov instability; Richtmyer (1960); Inoue et al. (2013)). $\Delta\rho_0 = 10$ % is, therefore, the characteristic level of inhomogeneity at which the speed of the dynamically condensing motion driven by the thermal instability (i.e., the sound speed of the UNM) is equal to the growth velocity of the shock-density inhomogeneity interaction. Given that the density inhomogeneity in the ISM typically ranges over many orders of magnitude (Armstrong et al., 1995, ; i.e., $\Delta\rho_0 > 10$ %), our results essentially suggest that most of the observed supersonic turbulence in molecular clouds may originate in the shock-density inhomogeneity interaction, which prevents the dynamical condensation purely by the thermal instability and keep the CNM mass fraction less

than 50 %.

To verify this formation mechanism of molecular clouds, it is crucial to observe 1) the probability distribution of density (or column density) of the pre-shock HI gas accreting onto molecular clouds, and 2) the mass fraction and velocity dispersion of HI gas within molecular clouds. Our simulation results from Kobayashi et al. (2020) indicate that the requirement of the spatial resolution and velocity is, ideally, 0.02 pc and 1.0 km s^{-1}, with which one cane probe the clumpy density structure (e.g., shown in Figure 2) and the level of turbulence.

Many previous surveys have conducted HI emission mapping by single dish and interferometer telescopes (e.g., Kalberla et al., 2005), and observational attempts has recently started to separate the multiphase structures into the WNM, UNM, and CNM (Kalberla & Haud, 2018). The ngVLA Band 1 capability of its high angular/spectral resolution and high sensitivity will enable us to access such detailed structure of HI gas inside/outside molecular clouds, mostly towards low-mass clouds in the Solar neighborhood (André et al., 2010). In the case of the Aquila rift cloud at the distance of 260 pc, as an example, the *Herschel* Gould Belt Survey reveal filamentary stuctures that host prestellar cores. To reveal the HI gas strcture surrounding these filaments, the ngVLA Band 1 is able to mosaic the main filament region (2 pc × 2 pc fields) in 40 hours, where each single pointing costs ~ 20 sec with the 7.7″ resolution (~ 0.02 pc) over 1 km s^{-1} line width to achieve the rms noise of 13 K. Besides such an emission observation, the absorption of HI combined with CO observations (Band 6) would also play an important role to reveal dark molecular clouds in such star-forming regions (e.g., Zuo et al., 2018), becuase the fraction of CNM in the pre-shock HI gas may alter the degree of turbulence driven in molecular clouds.

4. Macroscopic Viewpoint: Bulk properties of HI gas

Among molecular clouds, massive molecular clouds $\gtrsim 10^5$ M$_\odot$ host most of massive stars, imposing an important initial condition of galactic star formation. The population of such massive clouds is also important to observationally estimate the typical cloud lifetime (Koda et al., 2009; Meidt et al., 2015; Kobayashi et al., 2017, 2018). Massive molecular clumps are often observed in high-redshift star-forming galaxies as well (Tadaki et al., 2018).

The formation of massive molecular clouds require drastic mass accretion, which cannot be easily achieved by a simple extension of converging flows. For example, it requires that flows continue more than 10 Myr with the gas density of at least a few cm^{-3} and with the speed of more than 10 km s^{-1} (Heitsch et al., 2006), which is difficult by a single supernova and likely need the aid of large-scale flow (e.g., galactic spirals (Kim, Kim, & Ostriker (2020)), HI gas accretion from galactic halos and galaxy mergers). In addition, extremely massive ones $\gtrsim 10^6$ M$_\odot$ are likely remnant clouds that luckily survive from feedback processes such as stellar feedback and galactic shear motion (Herrera et al., 2020).

There are already observational and theoretical investigations suggesting the importance of such a drastic accumulation of HI gas. For example, a massive molecular cloud complex exists at the intersection of a spiral arm and the galactic bar

(W43; Kohno et al., 2020), which is surrounded by ambient H I gas (Nguyen Luong et al., 2011). Tidal interaction of the Magellanic clouds (Tsuge et al., 2020) induce massive compact clouds who host a young massive star cluster (Maeda, Inoue, & Fukui, 2021).

The Atacama Large Millimeter/Submillimeter Array (ALMA) started to reveal the inner structure of massive molecular clouds in relatively nearby galaxies (e.g., Galaxy M33; Muraoka et al. (2020); Tokuda et al. (2019), Kondo et al. submitted). With complementary surveys of H I gas, they suggest that those massive molecular clouds are formed by large-scale H I accumulation such as galactic spiral shocks, H I gas accretion (tidal interaction) from Galaxy M31 (Tachihara et al., 2018). The level of star formation activity differs between massive clouds, where the property of accreting H I gas may be responsible for such variety in star formation.

One way to investigate the dependence of star formation activity on the H I gas property is to observe the detailed H I gas structure associated with massive clouds in the Milky Way galaxy, similar to low-mass clouds but with limited pointings. In the case of W43, one of the most massive molecular cloud complexes in the Milky Way galaxy ($\sim 10^7$ M$_\odot$), it is located at 5.5 kpc and surrounded by diffuse H I gas (Kohno et al., 2020; Nguyen Luong et al., 2011). Albeit a single pointing with the maximum recoverable scale of 5.3 pc, the ngVLA Band 1 towards W43 will achieve the rms noise ~ 40 K in a single field with 48 hours integration with the $0.36''$ resolution (~ 0.02 pc) over 2 km s^{-1} line width. Such distance massive clouds may suffer from the line-of-sight contamination, but the kinematic distance estimation based on CO observations in Band 6 would mitigate this contamination (Roman-Duval et al., 2009) where CO is spatially correlated more with CNM than with WNM (Tachihara et al., 2018). Another possibility is targeting at clouds less-massive than W43 but with the less line-of-sight contamination expected (e.g., Maddalena's cloud, Cygnus OB7).

An alternative way is to investigate star-forming regions in the outer galaxy where H I gas accreting from the galactic halo directly trigger ongoing star formation with a <1 Myr timescale (Izumi et al., 2014). Such investigations in the outer galaxy can be also a hint to understand the cold accretion at high-redsfhit galaxies (Dekel & Birnboim, 2006). In the case of The Digel Cloud 1 at the distance of ~ 16 kpc, albeit a single pointing with the maximum recoverable scale of 150 pc, the ngVLA Band 1 towards the Digel Cloud 1 will achieve the rms noise becomes about 13 K in a single field with 48 hours integration with the $0.6''$ resolution (~ 0.1 pc) over 2 km s^{-1} line width.

Although the spatial resolution is limited, the ngVLA is also able to mosaic H I gas in nearby galaxies. For example, it covers the central region of GMC-8 in Galaxy M33 (50 pc $\times$ 50 pc fields) in 75 hours, where each single pointing costs ~ 3 hours with the $1.2''$ resolution (~ 10 pc) over 3 km s^{-1} line width to achieve the rms noise of 14 K. The ngVLA is, therefore, promising to reveal the formation mechanism of massive clouds by such a combination of high-resolution observations within the Milky Way and low-resolution observations of extragalactic H I.

5. Summary

The ngVLA becomes a complementary observatory of ALMA to observe the northern sky. Its capability of high angular/spectral resolution is promising to probe the inner density/velocity structure of H I gas outside/inside molecular clouds with a ~ 0.02 pc resolution in the solar neighborhood and with a ~ 10 pc resolution towards nearby galaxies. Complementary surveys in H I absorption and in CO emission will be a powerful method to obtain further information of the H I gas phases comprehensively from the WNM, UNM, and CNM, which will be the base of the understanding of molecular cloud life cycle including the origin of massive molecular clouds.

References

André, P., Men'shchikov, A., Bontemps, S. et al. 2010, A&A, 518, L102

André, P., Arzoumanian, D., Könyves, V., Shimajiri, Y., & Palmeirim, P. 2019, 629, L4

Audit, E., & Hennebelle, P. 2005, A&A, 433, 1

Armstrong, J. W., Rickett, B. J., & Spangler, S. R. 1995, ApJ, 443, 209

Baba, J., Morokuma-Matsui, K., & Saitoh, T. R. 2017, MNRAS, 464, 246

CaroCarroll-Nellenback, J. J., Frank, A., & Heitsch, F. 2014, ApJ, 790, 37

Dekel, A., & Birnboim, Y. 2006, MNRAS, 368, 2

Field, G. B. 1965, ApJ, 142, 531

Fukui, Y., Tsuge, K., Sano, H., Bekki, K., Yozin, C., Tachihara, K., & Inoue, T. 2017, PASJ, 69L, 5

Fukui, Y., Hayakawa, T., Inoue, T., et al. 2018, ApJ, 860, 33

Heiles, C., & Troland, T. H. 2003a, ApJS, 145, 329

Heiles, C., & Troland, T. H. 2003b, ApJ, 586, 1067

Heitsch, F., Burkert, A., Hartmann, L. W., Slyz, A. D., & Devriendt, J. E. G. 2005, ApJL, 633, L113

Heitsch, F., Slyz, A. D., Devriendt, J. E. G., Hartmann, L. W., & Burkert, A. 2006, ApJ, 648, 1052

Hennebelle, P., & Pérault, M. 1999, A&A, 351, 309

Hennebelle, P., Banerjee, R., Vázquez-Semadeni, E., Klessen, R. S., & Audit, E. 2008, A&A, 486, L43

Herrera, C. N., Pety, J., Hughes, A., 2020 A&A, 634A, 121

Heyer, M. & Dame, T. M. 2015, ARA&A, 26, 53

Inoue, T., & Inutsuka, S.. 2008, ApJ, 687, 303

Inoue, T., & Inutsuka, S.. 2012, ApJ, 759, 35

Inoue, T., Yamazaki, R., Inutsuka, S., & Fukui, Y., 2012, ApJ, 744, 71

Inoue, T., Shimoda, J., Ohira, Y., & Yamazaki, R. 2013, ApJL, 772, L20

Inoue, T., Hennebelle, P., Fukui, Y., Matsumoto, T., Iwasaki, K., & Inutsuka, S. 2018, PASJ, 70 S53

Iwasaki, K., & Inutsuka, S. 2014, ApJ, 784, 115

Iwasaki, K., Tomida, K., Inoue, T., & Inutsuka, S. 2019, ApJ, 873, 6

Izumi, N., Kobayashi, N., Yasui, C. et al., 2014, ApJ, 795, 66

Kalberla, P. M. W., Burton, W. B., Hartmann, D., Arnal E. M., Bajaja, E., Morras, R., & Pöppel, W. G. L. 2005, A&A, 440, 775

Kalberla, P. M. W., & Haud, U. 2018, A&A, 619, 58

Kennicutt, R. C., & Evans, N. J. 2012, ARA&A, 50, 531

Kim, C.-G., & Ostriker, E. C. 2015, ApJ, 802, 99

Kim, W.-T., Kim, C.-G., & Ostriker, E. C. 2020, ApJ, 898, 35

Kobayashi, M. I. N., Inutsuka, S., Kobayashi, H., & Hasegawa, K. 2017, ApJ, 836, 175

Kobayashi, M. I. N., Kobayashi, H., Inutsuka, S., & Fukui, Y. 2018 PASJ, 70, S59

Kobayashi, M. I. N., Inoue, T., Inutsuka, S., Tomida, K., Iwasaki, K., & Tanaka K. E. I. 2020, ApJ, 90, 95

Koda, J., Scoville, N., Sawada, T. et al. 2009, ApJ, 700, 132

Kohno, M., Tachihara, K., Torii, K., et al. 2020, PASJ, 73, S129

Kolmogorov, A. 1941, DoSSR, 30, 301

Koyama, H., & Inutsuka, S. 2000, ApJ, 532, 980

Koyama, H., & Inutsuka, S. 2002, ApJL, 564, L97

Koyama, H., & Inutsuka, S. 2004, ApJL, 602, L25

Kumar, M. S. N., Palmeirim, P., Arzoumanian, D., & Inutsuka, S. 2020, A&A, 642, 87

Larson R. B. 1969, MNRAS, 145, 271

Maeda, R., Inoue, T., & Fukui, Y. 2021, arXiv:2011.11650

McCray, R., & Snow, T. P. J. 1979, ARA&A, 17, 213

McKee, C. F., & Ostriker, J. P. 1977, ApJ, 218, 148

Meidt, S. E., Hughes, A., Dobbs, C. L. et al. 2015, ApJ, 806, 72

Muraoka, K., Kondo, H., Tokuda, K., 2020 ApJ, 903, 94

Nguyen Luong, Q., Motte, F., Schuller, F. et al. 2011, A&A, 529A, 41

Peretto, N., Fuller, G. A., Duarte-Cabral, A., Avison, A., Hennebelle, P., Pineda, J. E., André, Ph., Bontemps, S., Motte, F., Schneider, N., & Molinari, S. 2013, A&A, 555, 112

Richtmyer, R. D. 1960, Commun. Pure Appl. Math., 13, 297

Roman-Duval, J., Jackson, J. M., Heyer, M., 2009 ApJ, 699, 1153

Schneider, N., Bontemps, S., Motte, F., et al. 2016, A&A, 587, A74

Tachihara, K., Gratier, P., Sano, H., et al. 2018, PASJ, 70, S52

Tachihara, K., Fukui, Y., Hayakawa, T., & Inoue, T. 2018, arXiv:1811.02224

Tadaki, K., Iono, D., Yun, M. S. 2018, Nature, 560, 613

Tsuge, K., Sano, H., Tachihara, K. et al. 2020, arXiv:2010.08816

Tumlinson, J., Peeples, M. S., & Werk, J. K. 2017, ARA&A, 55, 389

Tokuda, K., Muraoka, K., Kondo, H. et al. 2020, ApJ, 896, 36

Valdivia, V., Hennebelle, P., Gérin, M., & Lesaffre, P. 2016, A&A, 587, A76

Vázquez-Semadeni, E., Ryu, D., Passot, T., González, R. F., & Gazol, A. 2006, ApJ, 643, 245

Wolfire, M. G., Hollenbach, D., McKee, C. F., Tielens, A. G. G. M., & Bakes, E. L. O. 1995, ApJ, 443, 152

Zuo, P., Li, D., Peek, J. E. G. 2018, ApJ, 867, 13